J Nanopart Res (2013) 15:1769
DOI 10.1007/s11051-013-1769-0

RESEARCH PAPER

Human serum albumin interactions with C_{60} fullerene studied by spectroscopy, small-angle neutron scattering, and molecular dynamics simulations

Song Li · Xiongce Zhao · Yiming Mo · Peter T. Cummings · William T. Heller

Received: 9 February 2013 / Accepted: 31 May 2013

Abstract Concern about the toxicity of engineered nanoparticles, such as the prototypical nanomaterial C_{60} fullerene, continues to grow. While, evidence continues to mount that C_{60} and its derivatives may pose health hazards, the specific molecular interactions of these particles with biological macromolecules require further investigation. In this article, we report combined experimental and theoretical studies on the interaction of one of the most prevalent proteins in the human body, human serum albumin (HSA), with C_{60} in an aqueous environment. The C_{60}–HSA interaction was probed by circular dichroism (CD) spectroscopy, small-angle neutron scattering (SANS), and atomistic molecular dynamics (MD) simulations to understand C_{60}-driven changes in the structure of HSA in solution. The CD spectroscopy demonstrates that the secondary structure of the protein decreases in α-helical content in response to the presence of C_{60} (0.68 nm in diameter). Similarly, C_{60} produces subtle changes in the solution conformation of HSA (an 8.0 nm × 3.8 nm protein), as evidenced by the SANS data and MD simulations, but the data do not indicate that C_{60} changes the oligomerization state of the protein, such as by inducing aggregation. The results demonstrate that the interaction is not highly disruptive to the protein in a manner that would prevent it from performing its physiological function.

Electronic supplementary material The online version of this article (doi:10.1007/s11051-013-1769-0) contains supplementary material, which is available to authorized users.

S. Li · P. T. Cummings
Department of Chemical and Biomolecular Engineering, Vanderbilt University, Nashville, TN 37235, USA

X. Zhao · P. T. Cummings (✉)
Center for Nanophase Materials Sciences, Oak Ridge National Laboratory, Oak Ridge, TN 37831, USA
e-mail: cummingspt@ornl.gov
URL: http://cnms.ornl.gov

Present Address:
X. Zhao
NIDDK, National Institutes of Health, Bethesda, MD 20892, USA

Y. Mo · W. T. Heller
Center for Structural Molecular Biology, Oak Ridge National Laboratory, Oak Ridge, TN 37831, USA

Y. Mo · W. T. Heller
Chemical Sciences Division, Oak Ridge National Laboratory, Oak Ridge, TN 37831, USA

Present Address:
Y. Mo
Institute of Agriculture, University of Tennessee, 109 McCord Hall, Knoxville, TN 37996, USA

W. T. Heller (✉)
Biology and Soft Matter Division, Oak Ridge National Laboratory, Oak Ridge, TN 37831, USA
e-mail: hellerwt@ornl.gov
URL: http://neutrons.ornl.gov

Published online: 21 June 2013

Keywords Fullerene · Serum albumin · Nanotoxicity · Small-angle neutron scattering · Molecular dynamics simulation

Introduction

The fullerene C_{60} (Kroto et al. 1985) was one of the first extensively-studied nanoparticles, and served as the prototypic building block that drove the explosive growth of the nanosciences. Fullerene derivatives, which are true macromolecular nanoparticles, have been studied for biological and pharmacological applications (Bosi et al. 2003a,b). For instance, functionalized C_{60} was proposed as an HIV protease inhibitor, (Friedman et al. 1993a,b ; Sijbesma et al. 1993) a photosensitizer for cancer treatment, (Tokuyama et al. 1993), and a delivery agent for gene therapy (Sitharaman et al. 2008; Raoof et al. 2012; Xu et al. 2012). While, the incredible promise of nanomaterials continues to drive research in this exciting field, consumer groups are increasingly concerned about the health effects of nanomaterials, leading to calls for the labeling of nanoparticle-containing products as potentially hazardous. (Using nanotechnology: What must be done, (Consumer Reports 2007)).

In the case of C_{60}, the debate about its health hazards, as well as those of related carbon nanomaterials, has intensified as evidence mounts on both sides of the debate. On one hand, several studies suggest that non-functionalized C_{60} is not acutely or is subacutely toxic to higher organisms, and may even be beneficial (Nelson et al. 1993; Scrivens et al. 1994; Gharbi et al. 2005; Baati et al. 2012). Dermal application of C_{60} was not demonstrated to be either toxic or cancerous in mice (Nelson et al. 1993). Aqueous suspensions of C_{60} were also found to be nontoxic to rats and indicated that the fullerenes protected against free-radical damage to the liver (Gharbi et al. 2005). While, it was found that incubation of C_{60} with isolated human keratinocytes resulted in cellular uptake of the nanoparticles, no evidence of toxicity was observed (Scrivens et al. 1994). A recent in vivo study in rats demonstrated that oral administration of C_{60} doubled the lifespan of the rats in the absence of chronic toxicity due to its attenuation of the oxidative stress (Baati et al. 2012). Similarly, C_{60} solubilized with polyvinylpyrrolidone did not cause hemolysis (Yamakoshi et al. 1994). Further, C_{60} was reported as a promising anti-amyloid agent that prevents in vitro accumulation of the amyloid-β_{25-35} peptide fragment (Makarova et al. 2012). These results help to drive the continued development of fullerene-based materials for biomedical applications.

In contrast, several studies have reported significant toxicity for C_{60}. Fullerene exposure was reported to produce oxidative stress in the brains of fish through the formation of reactive oxygen species, (Oberdorster 2004) raising particular concern because the fullerene has created an effect across the blood–brain barrier. In addition to showing the potential for causing long-term health effects, the study demonstrated a negative impact of fullerene dispersion into the environment. It has also been reported that the viability of cultured human skin and liver cells dramatically decreased in response to C_{60} application (Sayes et al. 2004). The potential for inheritable effects resulting from fullerene damage to DNA, as evidenced from a study using human lymphocytes, (Dhawan et al. 2006) is a great concern. Computational studies support a strong interaction between fullerenes and DNA/RNA that induces a structural deformation capable of inhibiting function (Zhao et al. 2005; Zhao 2008; Xu et al. 2012). Clearly, additional experimental and computational studies are required to establish the toxicity of C_{60} and to elucidate the specific molecular interactions that drive the toxicology of non-functionalized C_{60}.

The toxicity of water-soluble fullerenes has also been studied. While, a dendritic C_{60} mono-adduct decreased the viability of human lymphocytes, a malonic acid C_{60} tris-adduct did not (Rancan et al. 2002). However, exposure to UVA and UVB light caused both forms to become toxic. Carboxylated and polyhydroxyl-C_{60} (fullerol) were found to be considerably less toxic than non-functionalized C_{60}, (Sayes et al. 2004) and a separate study showed that fullerol did not produce toxic levels of oxidative stress (Xia et al. 2006). In contrast, fullerol nanoparticles displayed dose-dependent cytotoxicity in human peripheral blood lymphocytes (Mrdanovic et al. 2012). Further, orally-introduced, water-soluble trimethylenemethane-functionalized C_{60} was found to be transported to the liver in rats, (Yamago et al. 1995) and intravenous introduction rapidly dispersed it throughout the body before longer-term residence in the liver took place. Intravenously administered *p*,*p*′-bis (2-amino-ethyl)-diphenyl-C_{60} did not show toxicity

(Schinazi et al. 1993) and was excreted by rats with a half-life of roughly 7 h (Rajagopalan et al. 1996).

Studies of fullerene toxicity are invaluable for identifying potential health issues associated with these important nanoparticles, but little work has been done to investigate specific molecular interactions that may take place in the body. Here, we present a study of the interaction of non-functionalized C_{60} with the protein human serum albumin (HSA) in aqueous solution, where free C_{60} forms colloidal aggregates, (Andrievsky et al. 2002) to characterize the interaction of C_{60} with a model, biologically-relevant protein. HSA, a single polypeptide chain of 585 amino acids, is the most abundant protein in human plasma and is involved in a variety of physiological functions, including blood pH and pressure maintenance, as well as binding small hydrophobic molecules. HSA was studied in the presence of C_{60} using a combination of circular dichroism (CD) spectroscopy, small-angle neutron scattering (SANS), and atomistic molecular dynamics (MD) simulations to determine the impact of the nanoparticle on the protein. The experiments and simulations demonstrate that the structure of the protein is altered by its interaction with C_{60}, but it does not unfold or aggregate. This study supports the possibility that C_{60} can interact with HSA in a manner that would not entirely negatively impact all aspects of its function.

Experimental

Chemicals and solutions

Essentially fatty acid-free HSA (catalog number A3782), Trizma hydrochloride, Trizma base, and C_{60} were purchase from Sigma-Aldrich (St. Louis, MO). All materials were used as provided. A stock solution of HSA was prepared by dissolving the protein in 20 mM tris buffer at pH 7.4. The final stock concentration, as determined by UV–Vis spectroscopy with a Shimadzu 2401-PC spectrophotometer, was 10.1 mg/mL (0.152 mM) for the SANS measurements. Concentrations of 5 and 8 mg/mL were used for spectroscopy measurements. A stock solution of C_{60} in toluene was made at 10.4 mM. Sample preparation at 1:2, 1:1, 2:1, and 4:1 C_{60}:HSA ratios followed a procedure comparable to a previously described method for preparing aqueous dispersions of C_{60} (Andrievsky et al. 2002). Briefly, an appropriate amount of C_{60} in toluene was added to the HSA stock solution, vortexed vigorously. The toluene was blown off under a stream of dry air. The higher C_{60}:HSA ratios required additional vortexing and evaporation time to remove the toluene. The toluene removal process significantly reduced the sample volume (up to 25 %), which was made up using deionized water to maintain the concentration of the proteins and buffer salts. These relatively small changes in concentration are not anticipated to have a negative impact on the structure or aggregation state of the protein because of the higher concentration at which it natively exists in the blood. The final concentration of the C_{60}:HSA samples were approximately, but not exactly, the same as the starting stock solution as a result of the sample preparation. Presence of C_{60} in the solution was confirmed by UV–Vis spectroscopy by measuring a difference spectrum directly in the aforementioned instrument, which is a dual-beam model that allowed for direct collection of a difference spectrum from HSA samples with and without C_{60}.

CD spectroscopy

CD spectroscopy measurements were carried out using a Jasco 810 spectropolarimeter over wavelengths ranging from 280 to 195 nm. Sample concentrations were 5 or 8 mg/mL, and a 1 mm path-length sample cell was used. Protein secondary structure content was evaluated using the set of basis spectra determined from proteins of known structure (Chang et al. 1978), which were obtained from the K2D webpages (http://www.embl-heidelberg.de/~andrade/k2d.html) (Andrade et al. 1993).

SANS data collection

SANS experiments were performed using the Bio-SANS instrument at the High Flux Isotope Reactor at Oak Ridge National Laboratory (Lynn et al. 2006), Sample-to-detector distances of 1.1 and 6.8 m were used for the measurements. The wavelength, λ, was set to 0.6 nm, and the wavelength spread, $\Delta\lambda/\lambda$ was 0.15. The configurations provided the necessary q-range of 0.1–2.0 nm^{-1} for fitting and comparison against the crystal structure of the protein, and provided sufficient additional higher-q data for determination of the correct background subtraction. Data were corrected

for detector sensitivity and buffer or buffer-C_{60} backgrounds, as appropriate, before being azimuthally averaged into $I(q)$ versus q, where $q = (4\pi\sin(\theta))/\lambda$ and 2θ is the scattering angle from the direct beam.

SANS data analysis

SANS data were analyzed according to Guinier for the radius of gyration, R_g, (Guinier and Fournet 1955), and for the distance distribution function, $P(r)$, which is related to $I(q)$ by Eq. 1.

$$P(r) = \frac{1}{2\pi^2}\int_0^\infty dq \cdot (qr) \cdot I(q) \cdot \sin(qr) \quad (1)$$

The indirect Fourier transform algorithm implemented in the software GNOM (Svergun 1992) was used to determine $P(r)$ and the maximum linear dimension, d_{max}, from the measured intensity profiles. Comparison of the scattering data to a model intensity profile calculated from the crystallographic structure of HSA (PDB ID: 1AO6 (Sugio et al. 1999)) was performed using the program ORNL_SAS. (Tjioe and Heller 2007).

Molecular dynamics simulation

All molecular dynamics simulations were performed using the NAMD package (Phillips et al. 2005). An all-atom Amber force field (Cornell et al. 1996) was employed for both HSA protein and C_{60}. The initial configuration of HSA was obtained from the RCSB Protein Data Bank (PDB ID: 1AO6 (Sugio et al. 1999)). A C_{60}:HSA complex docking study was performed to predict the possible binding sites in HSA using PATCHDOCK (Duhovny et al. 2002; Schneidman-Duhovny et al. 2005). The final, starting structure of the 4:1 C_{60}:HSA complex was assembled from the four highest-ranked unique binding sites of C_{60} on HSA found by PATCHDOCK (Duhovny et al. 2002; Schneidman-Duhovny et al. 2005). PATCHDOCK has been used for predicting protein–protein and protein–small molecules interactions previously, specifically for, including HSA–Virstatin (Chatterjee et al. 2012), HSA–C_{60} (Belgorodsky et al. 2005; Benyamini et al. 2006) interactions. It was also successfully used to explore the possible binding sites of β-lactoglobulin with four carboxyl-modified C_{60} derivatives, in which the four ligands were docked onto β-lactoglobulin one-by-one and the highest-scored structure was found to strongly agree with experiment (Belgorodsky et al. 2007). Free HSA and the 4:1 C_{60}:HSA complex were solvated in an explicit TIP3P water box and neutralized by adding Cl^- and Na^+ ions. The system was allowed to undergo energy minimization and equilibration under isothermal-isobaric ensemble conditions. The equilibration was examined by checking the fluctuation of temperature, potentials, and root mean square displacement (RMSD), as shown in the supplementary information (Figures S1 and S2). The box dimensions are approximately 10.0 nm × 8.8 nm × 10.6 nm. Periodic boundary conditions were applied in all three dimensions. The temperature was controlled by Langevin method and the constant pressure was achieved by Langevin piston Nose-Hoover method. All hydrogen-linked bonds were constrained at fixed lengths during the simulation using the SHAKE algorithm (Ryckaert et al. 1977). Non-bonded interactions were calculated with a 1.0 nm cutoff. The particle mesh Ewald method (Darden et al. 1993) was used for electrostatic interactions. After 0.2-ns energy minimization and 5-ns equilibration, the 32 ns production run employed a 2 fs timestep. The trajectory was saved every 2 ps. Trajectories for free HSA and the 4:1 C_{60}:HSA complex were then used to calculate secondary structure evolution using STRIDE program (Heinig and Frishman 2004) in visual molecular dynamics (VMD). The binding sites on HSA for C_{60} were identified as the amino acid residues within 0.7 nm from C_{60}. The same residues in binding sites for free HSA and 4:1 C_{60}:HSA complex were used for secondary structure content analysis, respectively. The solvent accessible surface area (SASA) was evaluated from the MD trajectories and the ensemble SANS intensity profile, and $P(r)$ were computed from the coordinates using ORNL_SAS (Tjioe and Heller 2007). The R_g values for both free HSA and 4:1 C_{60}:HSA complex were also directly computed for comparison with the SANS data.

Results and discussion

The UV–Vis spectra of the free HSA and the 4:1 C_{60}:HSA sample are shown in Fig. 1. Excess absorbance, which is small relative to the tryptophan absorption band of the protein at 280 nm, can be seen in the spectra of the 4:1 C_{60}:HSA sample. The difference

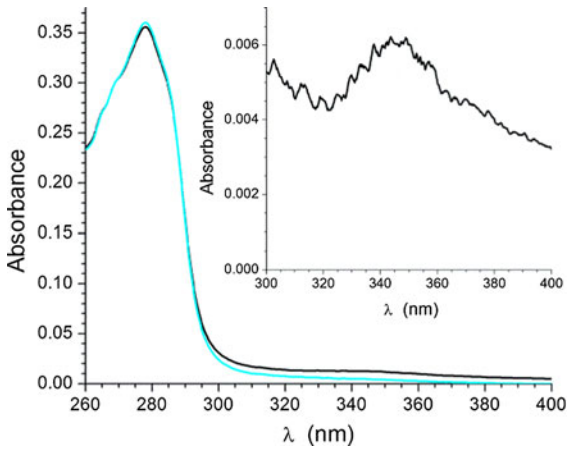

Fig. 1 UV-Vis spectra of 4:1 C_{60}:HSA (*cyan*) and free HSA (*black*) as-prepared samples. The difference spectrum, collecting using the free HSA sample as the background sample in the dual-beam spectrophotometer employed, is shown in the *inset* figure. No attempt was made to normalize for slight differences in concentration beyond making of the evaporated water volume during toluene evaporation as described in the "Experimental" Section. (Color figure online)

between the spectra for the 4:1 C_{60}:HSA sample and the free HSA is shown in the inset of the figure over the wavelength range of 260–400 nm, which includes the tryptophan absorption of the protein and one absorption peak of the C_{60}. The peak in the difference spectra is at 345 nm, which is consistent with other measurements of aqueous, colloidal solutions of C_{60} (Andrievsky et al. 2002; Fortner et al. 2005). The position of this feature depends on the preparation method. A previous study utilizing a similar organic-solvent based method for preparing a protein-free aqueous C_{60} dispersion found the same peak position, compared to 355 nm for directly dissolving the nanoparticle in water (Liu et al. 2012). The authors of the aforementioned study speculated that the size distribution of the C_{60} aggregates may have produced the differences in UV–Vis absorption. The present results are in reasonable agreement with another study that directly dissolved C_{60} in water with bovine serum albumin, and found an absorption peak of 343 nm (Wu et al. 2011). The results indicate that the C_{60} in the presence of a serum albumin is in a comparable state regardless of whether or not an organic solvent is used, although the organic solvent may have impacted the results, as suggested by Liu et al.(2012).

The CD spectra for free HSA and the C_{60}:HSA samples are shown in Fig. 2. The spectra are consistent with a predominantly α-helical protein, as expected from the crystal structure of HSA (Sugio et al. 1999), and show subtle changes in response to the addition of C_{60}. Fitting the spectrum of the free HSA for secondary structure content yields 62 % α-helix, 21 % β-structure and 17 % random coil, all with uncertainties of a few percent, and is consistent in helical content with previous measurements of HSA near neutral pH (Dockal et al. 2000). As can be seen in the main plot and in the inset, where the curves are overlaid onto one another, there are differences in the CD spectra in response to the addition of C_{60} that can be most clearly seen as a slight strengthening of the negative band near 208 nm relative to that near 222 nm with increasing C_{60} concentration. Fitting the spectra for secondary structure content, as described in the "Experimental" Section, finds that for the 1:2 C_{60}:HSA, the secondary structure content becomes 56 % α-helix, 24 % β-structure and 20 % random coil. Considering the sub-stoichiometric amount of C_{60} present and the

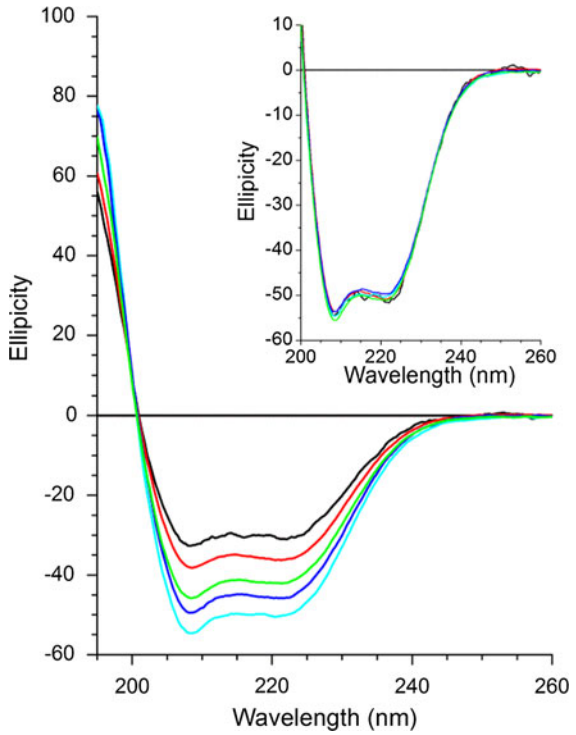

Fig. 2 CD spectra of C_{60}: HSA samples. The data for 1:2 (*red*), 1:1 (*green*), 2:1 (*blue*), and 4:1 (*cyan*) C_{60}:HSA and free HSA (*black*) in the main panel are not overlaid to allow for easy inspection. A relative normalization of the CD spectra at 222 nm was applied in the *inset* plot to highlight any changes in the spectra. (Color figure online)

possible colloidal nature of C_{60} in these samples, it is most appropriate to consider this to be an average secondary structure content, as the possibility exists that some HSA remains free in solution. At 1:1 C_{60}:HSA, the average secondary structure is 55 % α-helix, 22 % β-structure, and 23 % random coil. Similarly at 2:1 C_{60}:HSA, fitting the CD spectrum for protein secondary structure yields 56 % α-helix, 22 % β-structure, and 22 % random coil. A further change is observed when the C_{60}:HSA ratio increases to 4:1, resulting in 53 % α-helix, 23 % β-structure, and 24 % random coil. Data from a control experiment comparing the 4:1 C_{60}:HSA complex with HSA prepared in the same way with a C_{60}-free toluene solution are presented in the supplementary information (Figure S3). Exposure to toluene alone increased the β-structure content of the structure, and did not indicate significant denaturation of the structure during the process of toluene exposure and solvent evaporation. Considering that C_{60} can form colloidal aggregates in aqueous solution (Andrievsky et al. 2002; Fortner et al. 2005), it is possible that a fraction of the population of HSA is strongly altered by its association with C_{60}, while, the remainder may be in a free and unperturbed state. The CD data alone cannot resolve which state exists in the samples.

The C_{60}-driven changes in the CD spectra indicate that the conformational changes produced in HSA upon association with the nanoparticle are not large, such as might result from an extensive unfolding of the protein. Similar CD measurements of serum albumins (human and the closely-related bovine) associated with C_{60} have been performed previously (Song et al. 2011; Wu et al. 2011; Liu et al. 2012). At first glance, the results seem to be presenting a mixed message. For instance, Song et al. (2011) found that the α-helix of the structure increased, rather than decreased, upon binding the nanoparticle. The magnitude of the change is comparable to what is reported here. However, visual inspection of the data presented in the previous study finds that the spectra change in the same way, with an increase in the relative strength of the 208 nm band relative to the 222 nm band. In contrast, Wu et al. (2011) found visually similar spectral changes when bovine serum albumin associated with C_{60} under conditions suitable for solubilizing the nanoparticle and interpreted it as a loss of secondary structure, being presumably an increase in the random coil content, although no specifics were provided. These seemingly contradictory results can be reconciled by realizing that deconvolution of protein CD spectra for secondary structural content depends on the method and software employed. In all cases, the changes in the spectra, and thus protein conformation, appear consistent even if the interpretation differs. In contrast, Liu et al. (2012) observed what appeared to be qualitatively similar but lesser changes in the CD spectra of serum albumins associated with C_{60}, although the data are noisier and led the authors to conclude that no significant C_{60} dose-dependent changes in protein secondary structure took place. It is clear from the results viewed in aggregate that the nanoparticle does not cause large-scale changes in the secondary structure of the protein upon binding. It is interesting to note that the extent of the changes in CD spectra observed appears to be largely independent of whether the C_{60} was dissolved directly from powder or whether a C_{60} solution in toluene was employed.

The SANS data and Guinier fits are shown in Figs. 3 and 4, respectively, while $P(r)$ curves determined from the data fitting are shown in Fig. 5A. The SANS data and Guinier plots provide no indication of significant aggregation or the presence of a considerable population of high molecular weight particles, such as the protein-encapsulated C_{60} assemblies proposed in Scheme 1 of Wu et al. (2011), which are clearly larger than the particles indicated by the SANS data presented here, but are not so large as to be outside the range of length scales probed by the SANS measurements performed. The absence of high molecular weight species is most clear in the Fig. 4, which shows a linear Guinier region ($q \times R_g < 1.3$). The R_g determined from the free HSA data is 2.67 ± 0.12 nm, while the d_{max} determined from the $P(r)$ fitting was 8.50 ± 0.50 nm (Fig. 5A). The R_g values are unchanged to within the experimental uncertainty in response to the addition of C_{60}, being 2.67 ± 0.12, 2.62 ± 0.12, 2.68 ± 0.10, and 2.65 ± 0.09 nm for the 1:2, 1:1, 2:1, and 4:1 C_{60}:HSA samples, respectively, with corresponding d_{max} values of 8.25 ± 0.50, 8.25 ± 0.50, 8.50 ± 0.50, and 8.50 ± 0.50 nm, as found in the $P(r)$ fitting (Fig. 5A). These values are in reasonable agreement with a previous study of free HSA in aqueous solution, (Baker and Heller 2009; Heller 2013) although the samples reported in the earlier previous work (Baker and Heller 2009) may have contained ~10 % HSA dimers, resulting in a somewhat larger R_g. The SANS data demonstrate that no large-scale changes in tertiary structure or aggregation

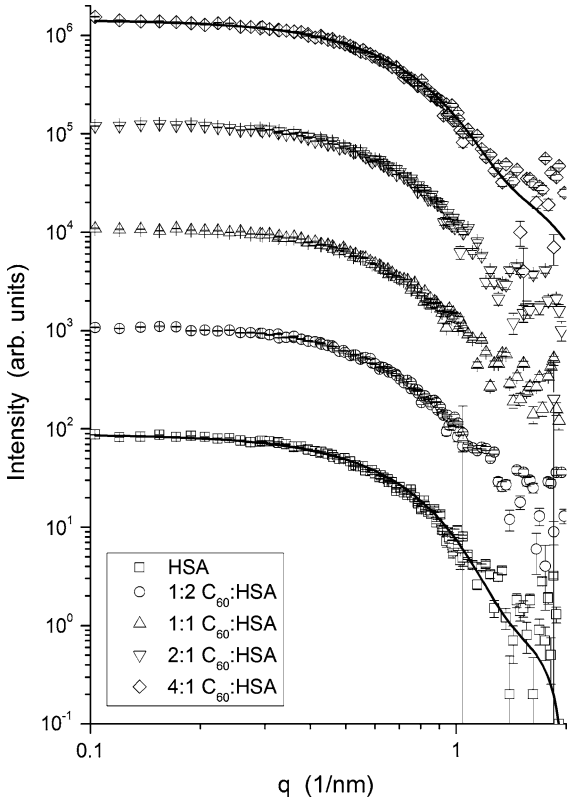

Fig. 3 SANS intensity profiles of C_{60}:HSA samples. The data for 1:2 (*circles*), 1:1 (*up triangles*), 2:1 (*down triangles*), and 4:1 (*diamonds*) C_{60}:HSA and free HSA (*squares*) have been offset for clarity. The *solid lines* are the intensity profiles calculated from the MD simulations of the free HSA and the 4:1 C_{60}:HSA complex. The differences at larger q-values are due to slight differences in the baseline that results from subtle differences in the background subtraction during data reduction

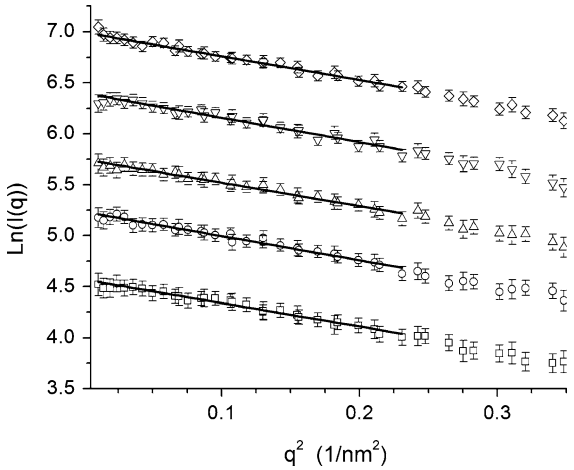

Fig. 4 Guinier plots of the C_{60}:HSA SANS data. The data for 1:2 (*circles*), 1:1 (*up triangles*), 2:1 (*down triangles*), and 4:1 (*diamonds*) C_{60}:HSA and free HSA (*squares*) have been offset for clarity. The *solid lines* are Guinier fits to the data

state have taken place. Some suggestion of a conformation change can be found by inspecting the $P(r)$ curves. However, the variations in the shape of the $P(r)$ curves are small, being at the edge of the uncertainties in the $P(r)$ fitting by GNOM (Svergun 1992). The extent of the changes in the global structure of the protein found by SANS are consistent with the changes in secondary structure found by CD spectroscopy (Fig. 2). Further, the choice of d_{max}, which is a fitting parameter left up to the user, can be subjective and can subtly impact the shape of $P(r)$. Taken together, the CD and SANS results make it possible to exclude the possibility that a portion of the HSA remains free and properly folded while, a population is associated with large colloidal C_{60} aggregates, as suggested by previous researchers (Song et al. 2011; Wu et al. 2011; Liu et al. 2012).

MD simulations were performed for free HSA and for the 4:1 C_{60}:HSA complex formed using the four highest ranked binding sites of C_{60} on HSA as determined using PATCHDOCK (Duhovny et al. 2002; Schneidman-Duhovny et al. 2005). The C_{60} sits within hydrophobic pockets on the surface of the protein, including in three locations along the cleft where the polypeptide chain folds into a heart-shape. The binding sites found are near the Myr2 and Myr4 myristic acid binding sites and the TIB2 tri-iodobenzoic acid binding site identified crystallographically (PDB ID:1BK5 and 1BKE (Curry et al. 1998)) and a different myristic acid binding site identified in another crystallographic study of the protein (PDB ID: 1E7G (Bhattacharya et al. 2000)). The Type I and Type II binding sites identified computationally (Benyamini et al. 2006) for C_{60} and carboxy-C_{60} are represented in the four sites identified here. Binding of C_{60} to HSA in vivo would involve competition between the nanoparticle and any fatty acids or other hydrophobic compounds, and would depend strongly on the specific compound occupying a site being competed for.

A snapshot of the simulation of the 4:1 C_{60}:HSA complex is shown in Fig. 6 in two views. The heart-shaped HSA structure observed crystallographically

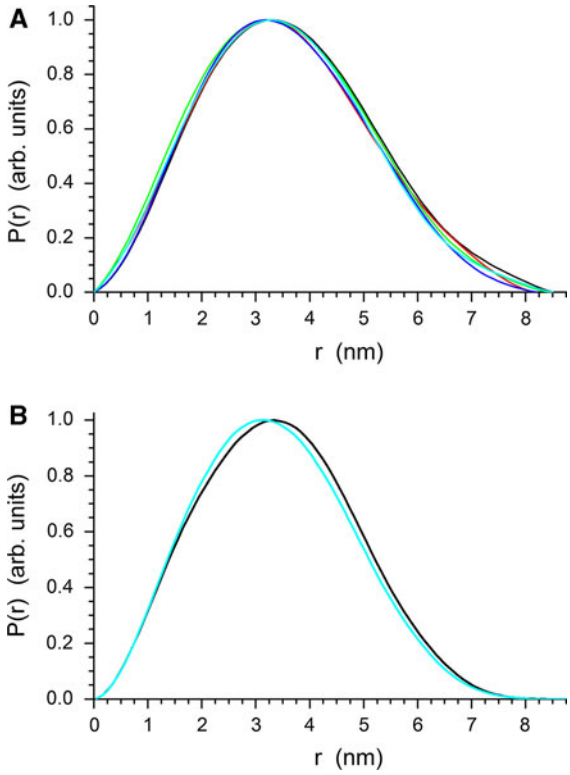

Fig. 5 **A** *P(r)* curves derived from the SANS data. The curves for 1:2 (*red*), 1:1 (*green*), 2:1 (*blue*), and 4:1 (*cyan*) C_{60}:HSA and free HSA (*black*) have been normalized to have equal value at the main peak. The *error bars* obtained during the *P(r)* fitting have been omitted for clarity, but are slightly larger than twice the line width. **B** *P*(*r*) curves calculated from the ensemble of MD simulation snapshots. The curves for 4:1 (*cyan*) C_{60}:HSA and free HSA (*black*) have been normalized to have equal value at the main peak. (Color figure online)

(Sugio et al. 1999) is not greatly disrupted by the bound C_{60} even after 32 ns of simulation. Interpretation of the trajectory for secondary structure content using the STRIDE program (Heinig and Frishman 2004), which is presented in Figure S4, shows little change in the relative contents of secondary structural elements over the course of the simulation, and subtle differences between the MD and experimental results can be attributed to the idealization inherent to the calculations relative to experiments performed. The secondary structure analysis of binding sites on free HSA and C_{60}:HSA complex, shown in Figure S5, suggests a slight decrease in α-helix content and increase in β-turn upon binding of C_{60}. Considering there is no obvious difference observed in the overall secondary structure contents between free HSA and C_{60}:HSA complex, it is reasonable to predict a corresponding subtle increase in α-helix and decrease in β-turn for the regions of HSA to which C_{60} binds. Therefore, the binding of C_{60} may cause the slight shift of secondary structure contents between the bound and unbound regions of HSA. SASA of the free and nanoparticle-bound protein is presented in Figures S6 and S7, and indicates that binding the nanoparticle does result in localized conformational changes that decrease the SASA and that such changes are primarily in the hydrophobic surface residues of HSA. Further, the global fold of the protein is not disrupted, which is consistent with the SANS results. The average R_g values for free HSA and 4:1 C_{60}:HSA from the MD simulation snapshots are 2.67 ± 0.01 and 2.65 ± 0.01 nm, respectively, which is in excellent agreement with the R_g determined from the SANS data for the free protein and 4:1 C_{60}:HSA complex. The MD results, being calculated from a single trajectory, cannot be considered a comprehensive examination of the conformational space available, but do support that the structure retains stability and overall fold rather than being driven to unfold. The MD simulations confirm the experimental findings that the binding of C_{60} to HSA does not cause a significant unfolding of the polypeptide chain from its native structure. The root mean square deviation (RMSD) relative to the initial structures (see Figure S2) are virtually identical (see Figure S2), suggesting that the crystal structure relaxes in the simulations. However, the average RMSD value calculated between simulation snapshots after equilibration of the free HSA and the 4:1 C_{60}:HSA complex, using SuperPose (Maiti et al. 2004), was determined to be 0.424 ± 0.010 nm, indicating significant atomic-level structural differences. The SANS intensity profiles calculated from the ensemble of structures in the snapshots of the simulations for free HSA and the 4:1 C_{60}:HSA complex are shown in Fig. 3 with the SANS data, while the *P*(*r*) curves determined from the simulations are presented in Fig. 5B. The SANS profiles calculated from the MD simulations agree very well with the data with primary discrepancies in the higher-*q* region, where the noise in the experimental SANS data is greatest. The *P*(*r*) curves calculated from the MD simulations show a slight shift of 0.2 nm in the position of the main peak to lower distances in response to C_{60}, but the d_{max} was unchanged. It should be noted that the simulation, which was performed using a specific complex at a well-defined binding stoichiometry

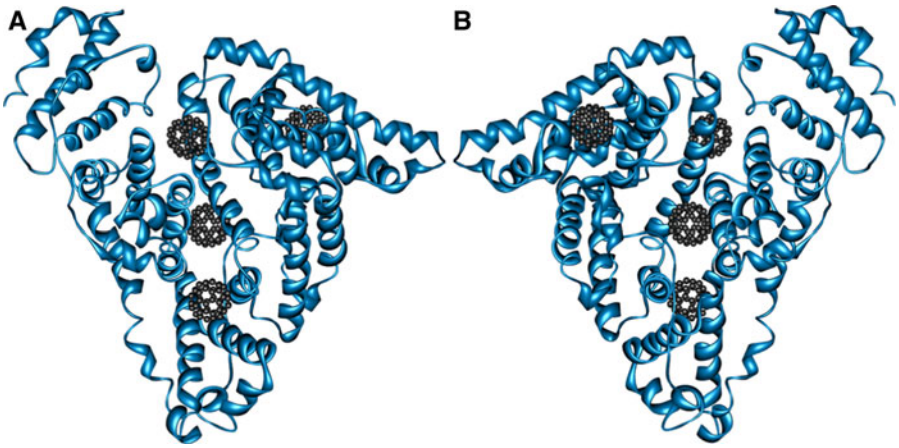

Fig. 6 Snapshot of simulation of the 4:1 C_{60}:HSA complex showing the location of the four most favorable binding sites determined by PATCHDOCK (Duhovny et al. 2002; Schneidman–Duhovny et al. 2005). Two views rotated 180° are presented (**A**, **B**) to show the binding sites on each face of HSA. Water molecules are omitted for clarity

identified by computational docking, only represents a small fraction of the potential conformational space available to the samples measured in the SANS experiments. However, the results are in qualitative agreement.

Conclusions

Here, the interaction of C_{60} with HSA, the most abundant protein found in blood plasma, was probed using CD spectroscopy, SANS and atomistic MD simulation. While no large colloidal aggregates of C_{60} were observed, a stable interaction between HSA and the nanoparticle was found. HSA plays an important biological role and is present in large quantities throughout the body. Its constant circulation and known interaction with molecules having hydrophobic moieties, such as fatty acids, makes it a candidate for transporting C_{60} and other hydrophobic nanoparticles. C_{60} is transported throughout the body to various organs, such as the liver (Gharbi et al. 2005), suggesting that transportation via the circulatory system is possible and could be facilitated by HSA through formation of a stable, non-covalently bound complex.

The current study shows that the HSA structure becomes slightly distorted when it interacts with C_{60}, as opposed to aggregating or unfolding. The present study expands on previous studies of C_{60} interacting with HSA in solution (Song et al. 2011; Wu et al. 2011; Liu et al. 2012) by providing insight into the conformation and aggregation state of the protein-nanoparticle complex in solution. Structural impacts of C_{60} of comparable scale were observed in computational studies of the binding of C_{60} to DNA (Zhao et al. 2005; Zhao 2008). The obvious consequences of unfolding are reduction or elimination of the function of a protein, and would raise health concerns about acute exposures to C_{60}. Maintaining a near-native HSA structure and oligomerization state would allow the nanoparticle–protein complex to move throughout the body, thereby providing an opportunity for C_{60} to accumulate in tissues not directly accessible through routes of entry, such as inhalation or ingestion.

Acknowledgments The authors thank Hugh M. O'Neill for access to the CD instrument. S.L., and P.T.C. acknowledge the use of computational facilities provided by the National Energy Research Scientific Computing Center (NERSC), which is supported by the Office of Science of the U.S. Department of Energy under Contract No. DE-AC02-05CH11231. Research at Oak Ridge National Laboratory's Center for Structural Molecular Biology (FWP ERKP291) was supported by the Office of Biological and Environmental Research of the U.S. Department of Energy. Research at Oak Ridge National Laboratory's High Flux Isotope Reactor was sponsored by the Scientific User Facilities Division, Office of Basic Energy Sciences, U.S. Department of Energy. Oak Ridge National Laboratory is managed by UT-Battelle, LLC for the U.S. Department of Energy under Contract No. DE-AC05-00OR22725.

References

Andrade MA, Chacon P, Merelo JJ, Moran F (1993) Evaluation of secondary structure of proteins from UV circular-dichroism spectra using an unsupervised learning neural-network. Protein Eng 6(4):383–390

Andrievsky GV, Klochkov VK, Bordyuh AB, Dovbeshko GI (2002) Comparative analysis of two aqueous-colloidal solutions of C-60 fullerene with help of FTIR reflectance and UV-Vis spectroscopy. Chem Phys Lett 364(1–2):8–17

Baati T, Bourasset F, Gharbi N, Njim L, Abderrabba M, Kerkeni A, Szwarc H, Moussa F (2012) The prolongation of the lifespan of rats by repeated oral administration of [C60] fullerene. Biomaterials 33(19):4936–4946

Baker GA, Heller WT (2009) Small-angle neutron scattering studies of model protein denaturation in aqueous solutions of the ionic liquid 1-butyl-3-methylimidazolium chloride. Chem Eng J 147(1):6–12. doi:10.1016/j.cej.2008.11.033

Belgorodsky B, Fadeev L, Ittah V, Benyamini H, Zelner S, Huppert D, Kotlyar AB, Gozin M (2005) Formation and characterization of stable human serum albumin—tris-malonic acid [C60]fullerene complex. Bioconjugate Chem 16(5):1058–1062. doi:10.1021/bc050103c

Belgorodsky B, Fadeev L, Kolsenik J, Gozin M (2007) Biodelivery of a fullerene derivative. Bioconjugate Chem 18(4):1095–1100. doi:10.1021/bc060363+

Benyamini H, Shulman-Peleg A, Wolfson HJ, Belgorodsky B, Fadeev L, Gozin M (2006) Interaction of C60–fullerene and carboxyfullerene with proteins: a docking and binding site alignment. Bioconjugate Chem 17(2):378–386. doi:10.1021/bc050299g

Bhattacharya AA, Grune T, Curry S (2000) Crystallographic analysis reveals common modes of binding of medium and long-chain fatty acids to human serum albumin. J Mol Biol 303(5):721–732. doi:10.1006/jmbi.2000.4158

Bosi S, Da Ros T, Spalluto G, Balzarini J, Prato M (2003a) Synthesis and anti-HIV properties of new water-soluble bis-functionalized [C60] fullerene derivatives. Bioorg Med Chem Lett 13(24):4437–4440. doi:10.1016/j.bmcl.2003.09.016

Bosi S, Da Ros T, Spalluto G, Prato M (2003b) Fullerene derivatives: an attractive tool for biological applications. Eur J Med Chem 38(11–12):913–923. doi:10.1016/j.ejmech.2003.09.005

Chang CT, Wu CSC, Yang JT (1978) Circular dichroic analysis of protein conformation—inclusion of beta-turns. Anal Biochem 91(1):13–31

Chatterjee T, Pal A, Dey S, Chatterjee BK, Chakrabarti P (2012) Interaction of virstatin with human serum albumin: spectroscopic analysis and molecular modeling. PLoS One 7(5):e37468. doi:10.1371/journal.pone.0037468

Cornell WD, Cieplak P, Bayly CI, Gould IR, Merz KM, Ferguson DM, Spellmeyer DC, Fox T, Caldwell JW, Kollman PA (1996) A second generation force field for the simulation of proteins, nucleic acids, and organic molecules (vol 117, pg 5179, 1995). J Am Chem Soc 118(9):2309

Curry S, Mandelkow H, Brick P, Franks N (1998) Crystal structure of human serum albumin complexed with fatty acid reveals an asymmetric distribution of binding sites. Nat Struct Biol 5(9):827–835. doi:10.1038/1869

Darden T, York D, Pederson L (1993) Particle mesh Ewald: an N·log(N) method for Ewald sums in large systems. J Chem Phys 98(12):10089

Dhawan A, Taurozzi JS, Pandey AK, Shan WQ, Miller SM, Hashsham SA, Tarabara VV (2006) Stable colloidal dispersions of C-60 fullerenes in water: evidence for genotoxicity. Environ Sci Technol 40(23):7394–7401. doi:10.1021/es0609708

Dockal M, Carter DC, Ruker F (2000) Conformational transitions of the three recombinant domains of human serum albumin depending on pH. J Biol Chem 275(5):3042–3050

Duhovny D, Nussinov R, Wolfson HJ (2002) Efficient unbound docking of rigid molecules. In: Guigo R, Gusfield D (eds) Algorithms in Bioinformatics, Proceedings, vol 2452. Lecture Notes in Computer Science. pp 185–200

Fortner JD, Lyon DY, Sayes CM, Boyd AM, Falkner JC, Hotze EM, Alemany LB, Tao YJ, Guo W, Ausman KD, Colvin VL, Hughes JB (2005) C-60 in water: nanocrystal formation and microbial response. Environ Sci Technol 39(11):4307–4316. doi:10.1021/es0498099n

Friedman SH, Decamp DL, Sijbesma RP, Srdanov G, Wudl F, Kenyon GL (1993a) Bucky-ball based inhibitors of the HIV protease—2nd-generation design and model studies. FASEB J 7(7):A1184

Friedman SH, Decamp DL, Sijbesma RP, Srdanov G, Wudl F, Kenyon GL (1993b) Inhibition of the HIV-1 protease by fullerene derivatives—model-building studies and experimental verification. J Am Chem Soc 115(15):6506–6509

Gharbi N, Pressac M, Hadchouel M, Szwarc H, Wilson SR, Moussa F (2005) [C60] Fullerene is a powerful antioxidant in vivo with no acute or subacute toxicity. Nano Lett 5(12):2578–2585. doi:10.1021/nl051866b

Guinier A, Fournet G (1955) Small-angle Scattering of X-rays. Wiley, New York

Heinig M, Frishman D (2004) STRIDE: a web server for secondary structure assignment from known atomic coordinates of proteins. Nucleic Acids Res 32:W500–W502. doi:10.1093/nar/gkh429

Heller WT (2013) Comparison of the thermal denaturing of human serum albumin in the presence of guanidine hydrochloride and 1-butyl-3-methylimidazolium ionic liquids. J Phys Chem B 117(8):2378–2383. doi:10.1021/jp400079p

Kroto HW, Heath JR, Obrien SC, Curl RF, Smalley RE (1985) C-60—buckminsterfullerene. Nature 318(6042):162–163

Liu SF, Sui Y, Guo K, Yin ZJ, Gao XB (2012) Spectroscopic study on the interaction of pristine C-60 and serum albumins in solution. Nanoscale Res Lett 7 7(1):433. doi:10.1186/1556-276x-7-433

Lynn GW, Heller W, Urban V, Wignall GD, Weiss K, Myles DAA (2006) Bio-SANS—a dedicated facility for neutron structural biology at oak ridge national laboratory. Phys B 385–86:880–882. doi:10.1016/j.physb.2006.05.133

Maiti R, Van Domselaar GH, Zhang H, Wishart DS (2004) SuperPose: a simple server for sophisticated structural superposition. Nucleic Acids Res 32:W590–W594. doi:10.1093/nar/gkh477

Makarova EG, Gordon RY, Podolski IY (2012) Fullerene C60 prevents neurotoxicity induced by intrahippocampal microinjection of amyloid-beta peptide. J Nanosci Nanotechnol 12(1):119–126

Mrdanovic JZ, ŠSolavic SV, Bogdanovic VV, Djordjevic AN, Bogdanovic GM, Injac RD, Rakocevic ZL (2012) Effects of fullerenol nano particles C60(OH)24 on micronuclei and chromosomal aberrations's frequency in peripheral blood lymphocytes. Dig J Nanomater and Bios 7(2):673–686

Nelson MA, Domann FE, Bowden GT, Hooser SB, Fernando Q, Carter DE (1993) Effects of acute and subchronic exposure of topically applied fullerene extracts on the mouse skin. Toxicol Ind Health 9(4):623–630

Oberdorster E (2004) Manufactured nanomaterials (fullerenes, C-60) induce oxidative stress in the brain of juvenile

largemouth bass. Environ Health Perspect 112(10): 1058–1062. doi:10.1289/ehp.7021

Phillips JC, Braun R, Wang W, Gumbart J, Tajkhorshid E, Villa E, Chipot C, Skeel RD, Kale L, Schulten K (2005) Scalable molecular dynamics with NAMD. J Comput Chem 26(16): 1781–1802. doi:10.1002/Jcc.20289

Rajagopalan P, Wudl F, Schinazi RF, Boudinot FD (1996) Pharmacokinetics of a water-soluble fullerene in rats. Antimicrob Agents Chemother 40(10):2262–2265

Rancan F, Rosan S, Boehm F, Cantrell A, Brellreich M, Schoenberger H, Hirsch A, Moussa F (2002) Cytotoxicity and photocytotoxicity of a dendritic C-60 mono-adduct and a malonic acid C-60 tris-adduct on Jurkat cells. J Photochem Photobiol B 67(3):157–162

Raoof M, Mackeyev Y, Cheney MA, Wilson LJ, Curley SA (2012) Internalization of C60 fullerenes into cancer cells with accumulation in the nucleus via the nuclear pore complex. Biomaterials 33(10):2952–2960

Ryckaert JP, Ciccotti G, Berendsen HJC (1977) Numerical integration of the cartesian equations of motion of a system with constraints: molecular dynamics of *n*-alkanes. J Comput Phys 23:327

Sayes CM, Fortner JD, Guo W, Lyon D, Boyd AM, Ausman KD, Tao YJ, Sitharaman B, Wilson LJ, Hughes JB, West JL, Colvin VL (2004) The differential cytotoxicity of water-soluble fullerenes. Nano Lett 4(10):1881–1887. doi: 10.1021/nl0489586

Schinazi RF, Sijbesma R, Srdanov G, Hill CL, Wudl F (1993) Synthesis and virucidal activity of a water-soluble, configurationally stable, derivatized C60 fullerene. Antimicrob Agents Chemother 37(8):1707–1710

Schneidman-Duhovny D, Inbar Y, Nussinov R, Wolfson HJ (2005) PatchDock and SymmDock: servers for rigid and symmetric docking. Nucleic Acids Res 33:W363–W367. doi:10.1093/nar/gki481

Scrivens WA, Tour JM, Creek KE, Pirisi L (1994) Synthesis of C-14-labeled C-60, its suspension in water, and its uptake by human keratinocytes. J Am Chem Soc 116(10): 4517–4518

Sijbesma R, Srdanov G, Wudl F, Castoro JA, Wilkins C, Friedman SH, Decamp DL, Kenyon GL (1993) Synthesis of a fullerene derivative for the inhibition of HIV enzymes. J Am Chem Soc 115(15):6510–6512

Sitharaman B, Zakharian TY, Saraf A, Misra P, Ashcroft J, Pan S, Pham QP, Mikos AG, Wilson LJ, Engler DA (2008) Water-soluble fullerene (C-60) derivatives as nonviral gene-delivery vectors. Mol Pharm 5(4):567–578. doi: 10.1021/mp700106w

Song MY, Liu SF, Yin JF, Wang HL (2011) Interaction of human serum album and C-60 aggregates in solution. Int J Mol Sci 12(8):4964–4974. doi:10.3390/ijms12084964

Sugio S, Kashima A, Mochizuki S, Noda M, Kobayashi K (1999) Crystal structure of human serum albumin at 2.5 angstrom resolution. Protein Eng 12(6):439–446

Svergun DI (1992) Determination of the Regularization Parameter in Indirect-Transform Methods Using Perceptual Criteria. J Appl Crystallogr 25:495–503

Tjioe E, Heller WT (2007) ORNL_SAS: software for calculation of small-angle scattering intensities of proteins and protein complexes. J Appl Crystallogr 40:782–785. doi: 10.1107/s002188980702420x

Tokuyama H, Yamago S, Nakamura E, Shiraki T, Sugiura Y (1993) Photoinduced Biochemical-Activity of Fullerene Carboxylic-Acid. J Am Chem Soc 115(17):7918–7919

Using nanotechnology: What must be done, (Consumer Reports, 2007). http://wwwconsumerreportsorg/cro/health/conditions-and-treatments/nanotechnology-7-07/what-must-be-done/0707_nano_what_1htm

Wu H, Lin LN, Wang P, Jiang SS, Dai Z, Zou XY (2011) Solubilization of pristine fullerene by the unfolding mechanism of bovine serum albumin for cytotoxic application. Chem Commun 47(38):10659–10661. doi:10.1039/c1cc13953c

Xia T, Kovochich M, Brant J, Hotze M, Sempf J, Oberley T, Sioutas C, Yeh JI, Wiesner MR, Nel AE (2006) Comparison of the abilities of ambient and manufactured nanoparticles to induce cellular toxicity according to an oxidative stress paradigm. Nano Lett 6(8):1794–1807. doi: 10.1021/nl061025k

Xu X, Wang X, Li Y, Wang Y, Yang L (2012) A large-scale association study for nanoparticle C60 uncovers mechanisms of nanotoxicity disrupting the native conformations of DNA/RNA. Nucleic Acids Res. doi:10.1093/nar/gks517

Yamago S, Tokuyama H, Nakamura E, Kikuchi K, Kananishi S, Sueki K, Nakahara H, Enomoto S, Ambe F (1995) In-vivo biological behavior of a water-miscible fullerene - C-14 labeling, absorption, distribution, excretion and acute toxicity. Chem Biol 2(6):385–389

Yamakoshi YN, Yagami T, Fukuhara K, Sueyoshi S, Miyata N (1994) Solubilization of Fullerenes into Water with Polyvinylpyrrolidone Applicable to Biological Tests. J Chem Soc-Chem Commun 4:517–518

Zhao XC (2008) Interaction of C-60 derivatives and ssDNA from simulations. J Phys Chem C 112(24):8898–8906. doi: 10.1021/jp801180w

Zhao XC, Striolo A, Cummings PT (2005) C-60 binds to and deforms nucleotides. Biophys J 89(6):3856–3862. doi: 10.1529/biophysj.105.064410